

Improving SuperBIT Mock Data with More Realistic Lenses

A. Mischel¹, A. Robertson^{2,*}, and E. Huff^{3,††}

¹ California Institute of Technology
e-mail: amischel@caltech.edu

² NASA Jet Propulsion Laboratory
e-mail: andrew.a.robertson@jpl.nasa.gov

³ NASA Jet Propulsion Laboratory
e-mail: eric.m.huff@jpl.nasa.gov

September 7, 2023

ABSTRACT

SuperBIT, a balloon-borne telescope launched in April 2023, has provided a unique opportunity to observe southern hemisphere galaxy clusters with a wide field-of-view in the near-infrared to near-UV range. By collecting data from weakly gravitationally lensed systems, it offers insights into the distribution of dark matter within these clusters. An analysis pipeline currently exists to infer mass distributions from the weakly gravitationally-lensed images, but its reliability is untested beyond simple cases. This project addresses the need for more rigorous testing of the analysis pipeline by utilizing the BAHAMAS simulations, which produce realistic-looking mass distributions of galaxy clusters. The focus of this project is to create realistic mock weak gravitationally lensed images by calculating the shear of various simulations. The final product is a repository which loads BAHAMAS simulations, calculates shear and convergence, and generates mock lensing images using randomly distributed background sources. By feeding these mock images to the analysis pipeline and checking if the correct mass distribution is inferred, we aim to provide higher confidence in the dark matter distributions from these galaxy clusters and any conclusions drawn about the nature of dark matter from these distributions.

Key words. weak gravitational lensing – shear – SuperBIT – BAHAMAS

1. Overview

Dark matter and dark energy are two of the most mysterious and elusive problems of the universe that have captured the attention of physicists for decades. In particular, researchers are interested in what particles dark matter could be made of, whether dark matter interacts with itself, and how these phenomena came into existence to begin with. Since neither interacts with light, researchers cannot study their properties directly and instead must turn to alternative methods for analyzing the effect these phenomena have on other cosmic objects that we can see.

One such method is gravitational lensing, an effect where light from a background source is deflected by the gravitational field of a foreground object, typically a galaxy or galaxy cluster. Since the deflection angle is dependent on the total mass of the foreground lens (including any dark matter), gravitational lensing combined with observations of the visible (baryonic) matter, can be used to map out dark matter. Gravitational lensing can be split into two qualitatively different regimes: strong and weak lensing. Strong gravitational lensing occurs at the center of large mass distributions, leading to multiple images of the same background source, as well as prominent “lensing arcs” (Bartelmann, 2010). Weak lensing, on the other hand, exists mainly at the outer regions of galaxy clusters and appears as slight distortions to the shapes of background galaxies. By analyzing both types of lensing, we can deduce the total mass distributions of entire galaxy clusters which helps to constrain cosmological parameters and test theories of dark matter to understand the expansion and structure of the universe (Bartelmann, 2010).

In the past, images of gravitational lenses have been taken using the Hubble Space Telescope, as well as ground-based telescopes. However, neither are ideal for studying weak gravitational lensing since the Hubble Space Telescope has a narrow field of view and ground-based telescope images experience blurred and fuzzy effects due to scattering of light in the atmosphere. To resolve these issues, JPL (along with Princeton, Durham and Toronto Universities) proposed SuperBIT, a balloon-borne telescope with a wider field of view than Hubble (Romualdez, 2018), which will look – in the near-infrared to the near-UV (Shaaban et. al, 2022) – at southern hemisphere galaxy clusters (Romualdez, 2018). SuperBIT successfully launched and recorded gravitational lens systems for 40 nights, so this project will help for the initial analyses of SuperBIT data.

Since the proposal of the SuperBIT balloon-borne telescope, the analysis pipeline for taking in images of weak gravitational lens systems and determining a mass distribution has been developed. To ensure the accuracy of this mass distribution determining algorithm, the lensing effects from simple mass distributions have been used to create “mock images” of what a hypothetical gravitational lens system would look like. However, these simplistic mass distributions do not produce mock lensed images that resemble realistic galaxy cluster lenses systems, and therefore are not comprehensive enough of a test for the image analysis code.

In this project, we work to develop work a code to generate mock lenses that input mass distributions generated from N-body simulations of the universe’s dark matter and baryonic matter over time. Such code will enable the generation of more realistic mock images, which can then be used to validate Super-

* Co-mentor

†† Co-mentor

BIT's gravitational lens analysis pipeline, allowing researchers to be confident in the accuracy of the inferred mass distributions.

2. Methods

2.1. General Lensing Theory

In a general lens system, the three main components are the observer, the lens, and the source (See Fig. 1). Since the distance from the observer to the lens (D_L) and the distance from the observer to the source (D_S) are so large relative to the size of the lens for most astronomical objects, the lens can be treated as a 2-dimensional screen, a limit called the "Thin Screen Approximation" (Narayan & Bartelmann, 1996). In this sense, the mass of the entire foreground lens can be projected onto a lens plane perpendicular to the line of sight. We define Σ , the projected surface mass density, or column density, as

$$\Sigma(\xi) = \int_{-\infty}^{\infty} \rho(\xi, z) dz \quad (1)$$

where ξ is some arbitrary 2-dimensional vector representing a location on the lens plane and z is the direction along the line of sight.

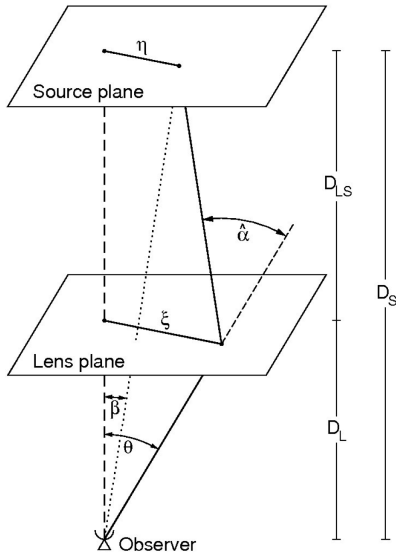


Fig. 1: Typical gravitational lensing system. η represents some arbitrary position on the source plane and ξ represents the location that place is mapped to on the lens plane. $\hat{\alpha}$ represents a scaled version of the deflection angle α , which is used to describe the mapping from the source to lens plane. (Figure from Bartelmann & Schneider, 2001)

For some arbitrary location on the lens plane, the deflection angle ($\hat{\alpha}$) is the angle the light path trajectory is bent when passing from a background source due to the presence of a lens. For a point mass with impact parameter for an unaffected light ray b (Gravitational Lensing Formalism, 2023), the magnitude of the deflection angle $\hat{\alpha}$ is

$$\hat{\alpha} = \frac{4GM}{c^2 b} \quad (2)$$

In lensing, $\hat{\alpha}$ is a two-dimensional vector pointing towards the direction of deflection and is dependent on the mass distribution of the lens. For more complicated mass distributions, the deflection angle is calculated by summing up contributions from all mass elements in the lens. The general formula for $\hat{\alpha}$ is

$$\hat{\alpha} = \frac{4G}{c^2} \int \frac{(\xi - \xi') \Sigma(\xi')}{|\xi - \xi'|} d^2 \xi' \quad (3)$$

where ξ is the location on the lens plane for which the deflection angle is being evaluated, and ξ' is the location on the lens plane for some lens mass element (Gravitational Lensing Formalism, 2023). Figure 2 better illustrates this relationship.

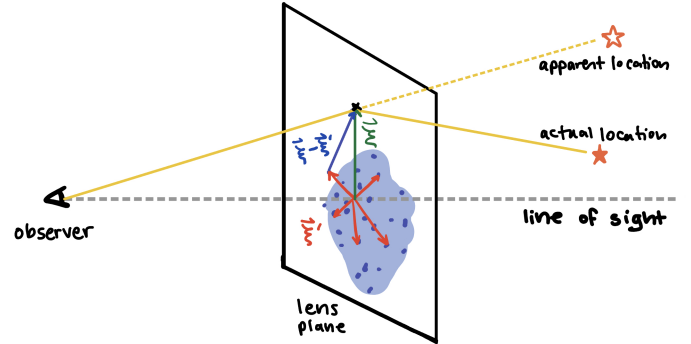


Fig. 2: Diagram of non-trivial lens mass distribution. ξ' represents a location of some mass element from the lens mass. ξ represents the location of evaluation of the deflection angle on the lens plane. By summing up the projected masses of the lens and scaling them by the distance from a given mass element to the point of evaluation ($\xi - \xi'$), along with other astrophysical constants, the deflection angle can be determined. (Figure from this project)

For most applications, it is much more convenient in lensing to define the reduced deflection angle α ,

$$\alpha(\theta) = \frac{D_{LS}}{D_S} \hat{\alpha}(\xi). \quad (4)$$

The reduced deflection angle α is the angle between the source's true location and where it appears to be due to lensing, as perceived by the observer. It should be noted that since the reduced deflection angle is measured from the observer, most lensing formalism uses θ when referring to a position on the lens plane, rather than ξ as this section has referred to up to this point. Assuming $|\theta|$ is in radians, the relationship between ξ and θ is

$$\xi = D_L \theta \quad (5)$$

We next define the critical surface density Σ_{crit} as

$$\Sigma_{\text{crit}} = \frac{c^2 D_S}{4\pi G D_{LS} D_L} \quad (6)$$

and the convergence, which is a scaled version of the projected mass density:

$$\kappa(\theta) = \frac{\Sigma(\theta)}{\Sigma_{\text{crit}}} \quad (7)$$

For $\kappa \geq 1$, multiple images of the background source appear in the lensed image. It should be noted that the value chosen for Σ_{crit} is somewhat arbitrary and changing the value of it would only affect the other quantities by the same scale factor¹.

We now define the lensing potential ψ as

$$\psi(\theta) = \frac{1}{\pi} \int \kappa(\theta') \ln |\theta - \theta'| d^2 \theta' \quad (8)$$

(Gravitational Lensing Formalism, 2023) such that the gradient of the potential is the deflection angle, and the Laplacian of the potential is twice the convergence:

$$\alpha(\theta) = \nabla \psi(\theta) \quad (9)$$

¹ More specifically, when producing mock lensed images, a different choice of the scaling factor would not affect the mock image, but the relationship that the ellipticity = shear/(1-convergence) of lensed originally perfect spheres would no longer hold.

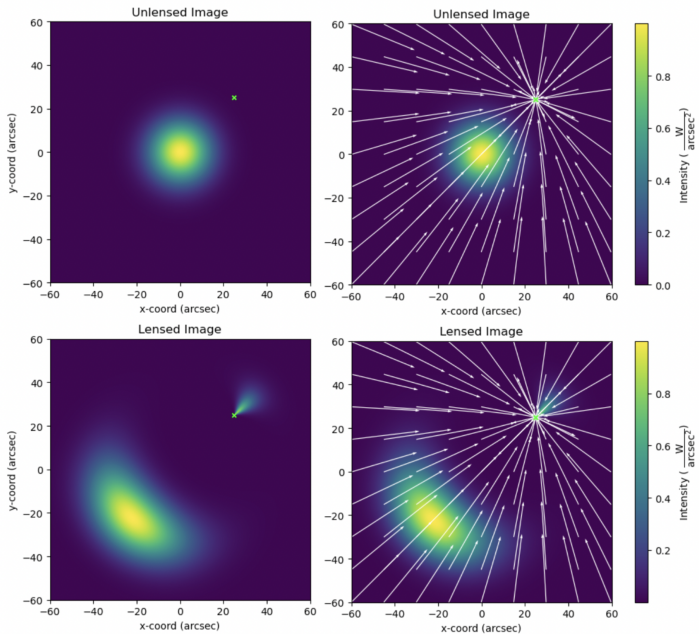


Fig. 3: Example of strong lensing. On the left is the unlensed and lensed image of a spherical background source with a Gaussian intensity distribution for the light. The lens is a singular isothermal sphere (SIS) centered on the neon green x. On the right is the same images with the deflection angle field plotted. For any given arrow in the lens plane, the head shows where the tail's light intensity is mapped from in the source plane. (Figure from this project)

$$\kappa(\theta) = \frac{1}{2} \nabla^2 \psi(\theta) \quad (10)$$

It is also useful to define the components of the shear, which involve second derivatives of the potential, similar to the convergence. These components are called γ_1 and γ_2 and are used in weak gravitational lensing (Narayan & Bartelmann, 1996). They are defined as

$$\gamma_1(\theta) = \frac{1}{2} \left(\frac{\partial^2 \psi}{\partial \theta_x^2} - \frac{\partial^2 \psi}{\partial \theta_y^2} \right) \quad (11)$$

$$\gamma_2(\theta) = \frac{\partial^2 \psi}{\partial \theta_x \partial \theta_y} \quad (12)$$

The deflection potential is also proportional to the projected Newtonian gravitational potential (Gravitational Lensing Formalism, 2023), which we define as ϕ .

$$\psi(\theta) = \frac{2D_{LS}}{D_S D_L c^2} \int \phi(\theta, z) dz \quad (13)$$

2.2. Weak Lensing Theory

For strong gravitational lens systems, calculating the deflection angle field is useful since the magnitude of the deflection angle field is large enough to produce changes in position of background sources. However, in the case of weak gravitational lensing, the background source is very distant, small, or far away from the line of sight, so both the deflection angle field and its gradient are small and approximations can be applied.

In contrast to strong lensing, which results in the formation of prominent arcs or multiple images, weak lensing manifests as subtle distortions in the source image (Narayan & Bartelmann, 1996). This effect is well illustrated in Figure 4.

In the limit of weak gravitational lensing, it is assumed that the convergence and shear are small and largely constant across

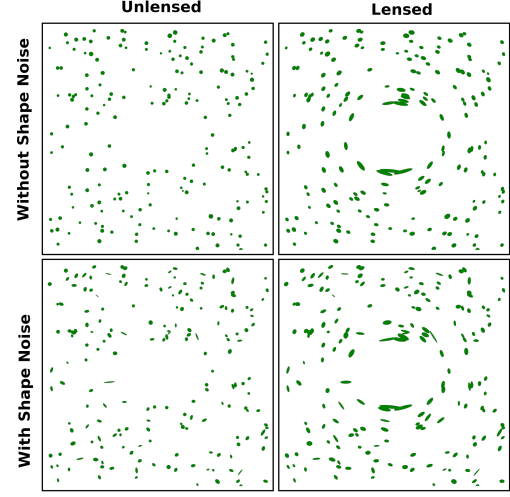


Fig. 4: Weak lensing diagram. The top row shows a random distribution of circular background sources and its unlensed and lensed images. The bottom row shows the same image as the top row but with shape noise of the background sources. As seen from the lensed image, the locations of the background sources is unchanged due to lensing, but the ellipticities of the background sources are affected and form a symmetric pattern around the lens mass with strength decreasing as distance from the lens increases. (Figure from Wikipedia, Weak Lensing Formalism)

the lensing map. Due to this, weak lensing approximates that each background source has one value for the convergence and one value for each shear component.

For the case of weak gravitational lensing, the convergence alone represents a magnification of the background source, while the magnitude of the shear ($\gamma = \sqrt{\gamma_1^2 + \gamma_2^2}$) represents the amount the background source is stretched (Narayan & Bartelmann, 1996). The components of shear can be rewritten from Equations 11 and 12 as

$$\gamma_1(\theta) = \gamma(\theta) \cos[2\phi(\theta)] \quad (14)$$

$$\gamma_2(\theta) = \gamma(\theta) \sin[2\phi(\theta)] \quad (15)$$

where ϕ represents the orientation of the stretched background source (not to be confused with how ϕ was previously defined as the Newtonian potential in Equation 13). The factor of 2 within the sine and cosine terms in Equations 14 and 15 are important. γ_1 represents a stretching or squeezing in the orthogonal direction, while γ_2 represents a stretching or squeezing along the 45° angle. For some intuition, consider a lensed background source (which was originally circular) whose major and minor axes lay along the orthogonal directions. An angle of 0° would make $\gamma_1 = \gamma$ and $\gamma_2 = 0$, which checks out with the way they are defined. Consider a different lensed background source whose major and minor axes lay along the 45° line. An angle of 0° would make the components of shear $\gamma_1 = 0$ and $\gamma_2 = \gamma$, which also checks out with the way they are defined. Figure 5 illustrates this well.

Using the definitions of convergence and shear, the Jacobian matrix A defining the lensing transformation from an unlensed to a lensed image can be written. The Jacobian matrix determines how a change in θ affects a change in β . It is written as follows (Gravitational Lensing Formalism, 2023):

$$A = (1 - \kappa) \begin{bmatrix} 1 & 0 \\ 0 & 1 \end{bmatrix} - \gamma \begin{bmatrix} \cos 2\phi & \sin 2\phi \\ \sin 2\phi & -\cos 2\phi \end{bmatrix} \quad (16)$$

Though the convergence and shear are related by taking second derivatives of the lensing potential, a more direct relationship can be found by using Fourier transformations. The general

	< 0	> 0
κ		
$\text{Re}[\gamma]$		
$\text{Im}[\gamma]$		

Fig. 5: Visual intuition for convergence and shear. κ represents the magnification of shear, while γ represents the stretching. In particular, γ_1 represents a stretching along the orthogonal direction, and γ_2 represents a stretching along the 45° direction. (Figure from Wikipedia, Weak Lensing Formalism)

formula for the inverse Fourier transform is

$$f(x) = \int_{-\infty}^{\infty} \hat{f}(\xi) e^{i2\pi\xi x} d\xi, \forall x \in \mathbb{R} \quad (17)$$

where ξ is the frequency and $\hat{f}(\xi)$ is the Fourier transform of $f(x)$. Therefore, the inverse Fourier transform of the lensing potential is

$$\psi(\theta_x, \theta_y) = \int_{-\infty}^{\infty} \hat{\psi}(k_x, k_y) e^{2\pi i(\theta_x k_x, \theta_y k_y)} dk_x dk_y \quad (18)$$

Taking different combinations of the second derivatives of $\psi(\theta_x, \theta_y)$ gives

$$\frac{\partial^2 \psi}{\partial \theta_x^2} = \int_{-\infty}^{\infty} (2\pi k_x)^2 \hat{\psi}(k_x, k_y) e^{2\pi i(\theta_x k_x, \theta_y k_y)} dk_x dk_y \quad (19)$$

$$\frac{\partial^2 \psi}{\partial \theta_y^2} = \int_{-\infty}^{\infty} (2\pi k_y)^2 \hat{\psi}(k_x, k_y) e^{2\pi i(\theta_x k_x, \theta_y k_y)} dk_x dk_y \quad (20)$$

$$\frac{\partial^2 \psi}{\partial \theta_x \partial \theta_y} = \int_{-\infty}^{\infty} (2\pi i)^2 k_x k_y \hat{\psi}(k_x, k_y) e^{2\pi i(\theta_x k_x, \theta_y k_y)} dk_x dk_y \quad (21)$$

Using Equation 10,

$$\begin{aligned} \kappa &= \frac{1}{2} \left(\frac{\partial^2 \psi}{\partial \theta_x^2} + \frac{\partial^2 \psi}{\partial \theta_y^2} \right) \\ &= \int_{-\infty}^{\infty} \frac{1}{2} (2\pi i)^2 (k_x^2 + k_y^2) \hat{\psi}(k_x, k_y) e^{2\pi i(\theta_x k_x, \theta_y k_y)} dk_x dk_y \end{aligned} \quad (22)$$

The inverse Fourier transform of the convergence is as follows.

$$\kappa(\theta_x, \theta_y) = \int_{-\infty}^{\infty} \hat{\kappa}(k_x, k_y) e^{2\pi i(\theta_x k_x, \theta_y k_y)} dk_x dk_y \quad (23)$$

Setting Equation 22 and 23 equal to each other,

$$\hat{\kappa}(k_x, k_y) = \frac{1}{2} (2\pi i)^2 (k_x^2 + k_y^2) \hat{\psi}(k_x, k_y) \quad (24)$$

A similar technique can be applied to γ_1 and γ_2 using Equations 11 and 12.

$$\hat{\gamma}_1(k_x, k_y) = \frac{1}{2} (2\pi i)^2 (k_x^2 - k_y^2) \hat{\psi}(k_x, k_y) \quad (25)$$

$$\hat{\gamma}_2(k_x, k_y) = (2\pi i)^2 k_x k_y \hat{\psi}(k_x, k_y) \quad (26)$$

Rearranging Equation 24 for ψ ,

$$\hat{\psi}(k_x, k_y) = \frac{\hat{\kappa}(k_x, k_y)}{\frac{1}{2} (2\pi i)^2 (k_x^2 - k_y^2)} \quad (27)$$

which can then be plugged into Equations 25 and 26, giving

$$\hat{\gamma}_1 = \frac{k_x^2 - k_y^2}{k_x^2 + k_y^2} \hat{\kappa} \quad (28)$$

$$\hat{\gamma}_2 = 2 \frac{k_x k_y}{k_x^2 + k_y^2} \hat{\kappa} \quad (29)$$

From this, we have derived two expressions relating the convergence to the components of shear.

To describe a weak lensing system, some use both the convergence and shear to show the lensed size of the background source and the amount and direction it is stretched, respectively (as seen in Figure 5). However, often more common is to characterize an image by the shear and magnification. Referring to the definition of A in Equation, the magnification μ is defined as (Narayan & Bartelmann, 1996):

$$\mu = \frac{1}{\det(A)} = \frac{1}{(1 - \kappa)^2 - \gamma^2} \quad (30)$$

2.3. BAHAMAS Simulations

To produce mock weak gravitational lens images that are compatible with the analysis pipeline, we developed a code to generate a map of the convergence and shear field for a generated mass distribution. We decided to use the BAHAMAS (BAryons and HALoes of MAssive Systems) simulations to generate these mass distributions.

The BAHAMAS Simulations are a host of large-scale N-body simulations of the universe's dark matter, stars, gas, and black hole content (McCarthy, 2017). These simulations attempt to provide high-resolution simulations on the galaxy cluster scale that can be used in a variety of astrophysical applications. Since the BAHAMAS simulations render the mass distributions of galaxy clusters, which make up most gravitational lenses, it was a good choice for making mock images.

The simulations store information on the positions of dark matter, stars, gas, and black hole particles as well as their associated masses. The zoom of each generated simulation and type of particle displayed can be chosen.

We loaded 20 simulations of galaxy clusters with all particle types and displayed them by creating a 2D histogram of the positions of all particles with their associated mass. An example of some of the plots of the masses of these particles is shown in Figures 8-11.

In order to use these simulations, we first calculated the Σ of each galaxy cluster by making the 2D histogram as mentioned previously. The value of Σ_{crit} was then calculated for given lens and source redshifts and the projected mass density was scaled by Σ_{crit} to calculate the convergence. Using equations 28 and 29 from the Weak Lensing Theory section, the Fourier transforms of γ_1 and γ_2 were calculated. An inverse Fourier transform was applied on both $\hat{\gamma}_1$ and $\hat{\gamma}_2$ in order to calculate the final values of γ_1 and γ_2 and the magnitude of γ . Finally, linear interpolation was used to create a function to find γ or its components at any given point within the simulation plot. Once the convergence and shear were calculated, another function was written to calculate μ , the magnification. Later functions were also written to plot the shear, convergence, and magnification fields.

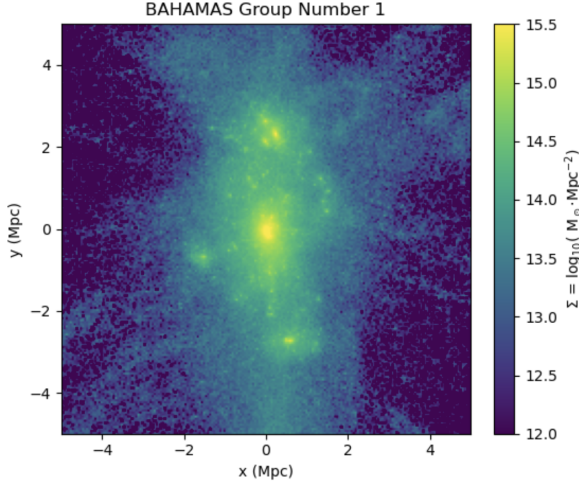


Fig. 6: BAHAMAS Simulation of a galaxy cluster plot of $\log_{10}(\Sigma)$.

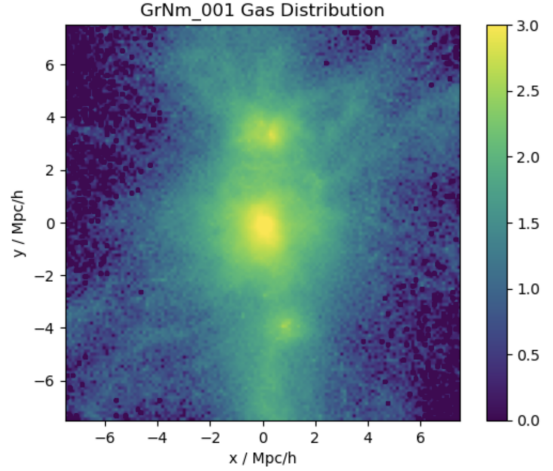


Fig. 9: BAHAMAS Simulation of a galaxy cluster with only the gas plotted.

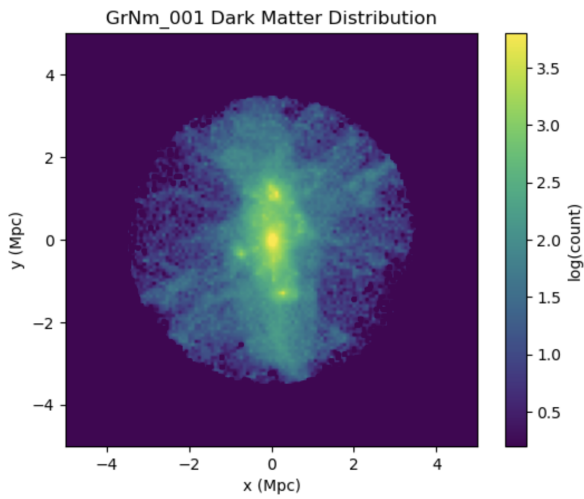


Fig. 7: BAHAMAS Simulation of a galaxy cluster with only the dark matter plotted.

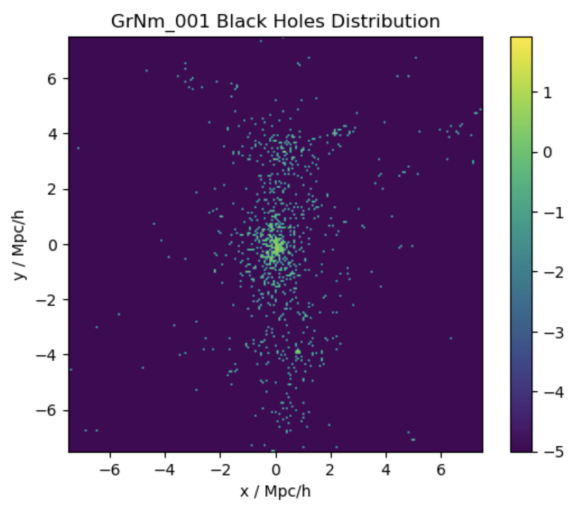


Fig. 10: BAHAMAS Simulation of a galaxy cluster with only the black holes plotted.

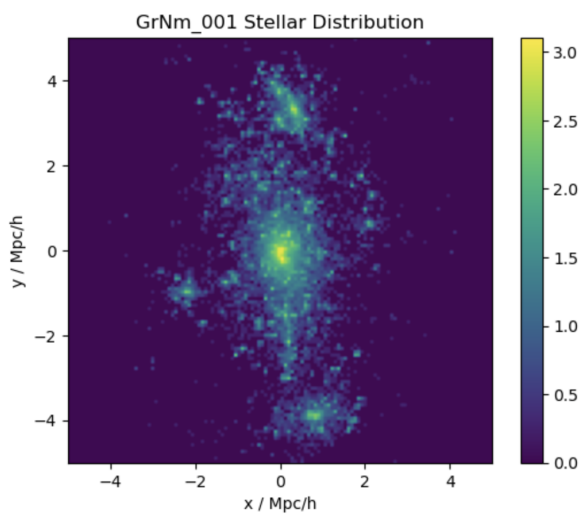


Fig. 8: BAHAMAS Simulation of a galaxy cluster with only the locations of stars plotted.

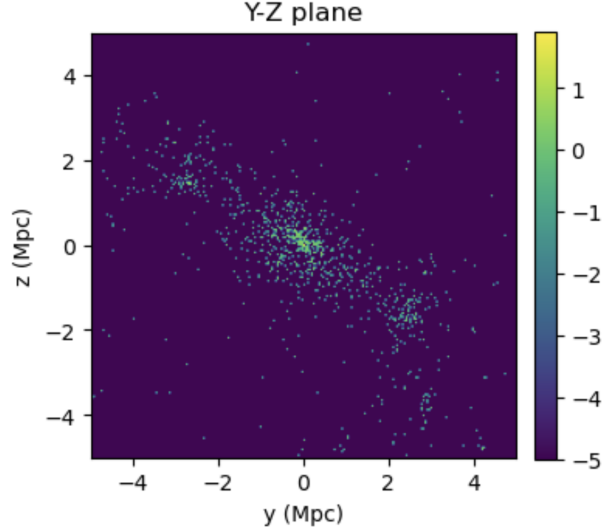


Fig. 11: BAHAMAS Simulation of a galaxy cluster showing the black holes plotted on the YZ plane (instead of XY).

3. Results

The final product for this project is a public GitHub repository capable of loading BAHAMAS simulations and calculating the convergence and shear of the simulated mass distribution. This repository is called BAHAMAS-mock-weak-lensing and can be accessed by this URL: <https://github.com/anyamischel/BAHAMAS-mock-weak-lensing>.

Within the repository are the following files:

1. README.md
2. requirements.txt
3. Lensing.py
4. Simulation.py
5. BHMsim.py
6. Running_BHM_Sims.py

as well as .ipynb versions of most of these files.

The main files in this repository are Lensing.py, Simulation.py, and BHMsim.py. Lensing.py and Simulation.py are python files that contain methods to calculate lensing and simulation properties to make the methods more organized. Lensing.py is responsible for all lensing-related calculations, such as that of Σ_{crit} , the convergence, and the shear components. Since the writing for Lensing.py began at the beginning of this project, it also includes methods to make calculations of strong lensing systems, including the Einstein ring radius, the deflection angle field due to a Singular Isothermal Sphere (SIS), and functions to generate mock sources with a Gaussian intensity distribution.

Simulation.py is responsible for taking a pre-loaded BAHAMAS simulation and calculating the Σ from it using the methods described in section 2.3. *BAHAMAS Simulations*.

BHMsim.py contains the class BHMsim, which is meant to represent a BAHAMAS simulation. When instantiating an object of the class, the user can input properties of the lensing system such as the lens redshift, the axes to view the simulation (XY, YZ, XZ), and the field-of-view the BAHAMAS simulation covers. Inside the class are methods to calculate the convergence and shear fields, and evaluate them at any point using linear interpolation for a given source redshift. Finally, BHMsim contains methods to plot the convergence, shear, and magnification with inputs that allow the user to choose the field-of-view of the final plots (default is the SuperBIT field-of-view). Users are also able to plot shear lines, which help visualize the direction the shear field stretches background sources.

Running_BHM_Sims.py was included as an example of how to instantiate an object of the BHMsim class and plot images of the convergence, shear, and magnification fields. README.md and requirements.txt contain information regarding the structure of the repository, how to use it, and the packages necessary to do so.

Displayed in Figures 12-14 are plots taken from Running_BHM_Sims.py with the first simulation (GrNm_001) from BAHAMAS_cutouts. Figure 12 and Figure 13 display the default convergence and shear plots, but Figure 13 displays the shear with shearlines turned on. The difference between a 'default' convergence or shear and the true convergence or shear is the source redshift, which only scales the value of the convergence or shear field. Due to this, changing the value of the source redshift and plotting the true convergence and shear would only affect the values on the colorbar, not the actual appearance of the image and thus a default source redshift of 1.0 was chosen for all convergence and shear plots. In Figure 13, the color of the

plot indicates the strength of the stretching of background galaxies, while the direction the shearlines point indicate the direction in which background sources would be stretched. Together, the color plot and shearlines help show that background sources closer to the center would be stretched stronger than sources further from the center and all background sources are stretched roughly radially around the center of the source. Figure 14 also displays the magnification (also with a default source redshift of 1.0) which forms an interesting ring shape toward the center of the plot.

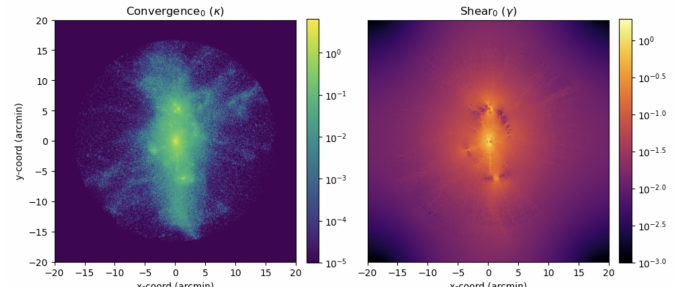


Fig. 12: BAHAMAS Simulation 1: logarithm of the convergence and shear.

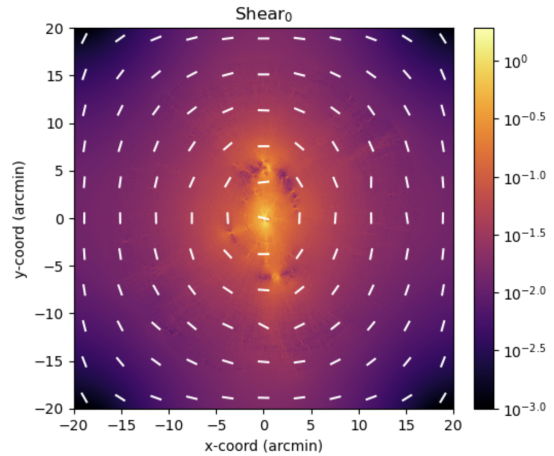


Fig. 13: BAHAMAS Simulation 1: logarithm of the shear with shearlines plotted. The length of all lines is fixed but the direction is controlled by the components of the shear.

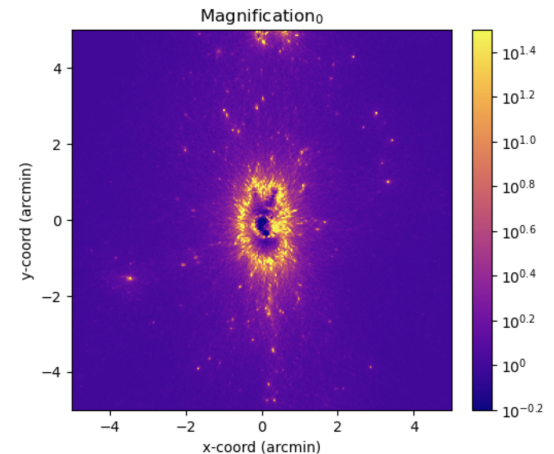


Fig. 14: BAHAMAS Simulation 1: logarithm of the magnification.

4. Conclusions

By using the shear and magnification plots of these 20 different simulations and having control over the field-of-view to match that of SuperBIT's, these plots should hopefully help improve the rigor of testing of the SuperBIT analysis pipeline. Since there are 20 unique simulations and 3 options for axes to view them from, there will be a total of 60 unique shear plots with associated mass distributions to feed into the pipeline.

Though these mock shear plots will be beneficial for testing the analysis pipeline with more realistic mass distributions, there are certainly still limitations to these images.

First, the `scipy` package used to compute the Fourier transform of the convergence does so by inputting an original image the size of the BAHAMAS simulation and then creating a grid of those images around it. However, this means that sharp edges arise since the convergence changes quickly at the edge of one of the grids to the next. To combat this, zero padding was incorporated. Zero padding adds a bunch of zeros around each grid to space them out, preventing the steep change in convergence between the edge of one simulation grid and its neighbor.

However, this method is still not perfect. Though the edge between simulation grids is no longer an issue, there is still a harsh edge between the edge of the simulation plot (with non-zero convergence) and the zero padding. Originally, the simulations were zoomed much further in to fit the size of the SuperBIT field-of-view. However, the size of the convergence was greatly expanded so the plot included the entire simulation and its edge. Since the mass distribution in the simulation is a projected mass distribution, and the simulation is a sphere, the outermost edge of the simulation is very thin along the line of sight, meaning the projected mass density is much smaller there compared to the center of the simulation. This way, by including the edge of the simulation in the convergence plot, the dropoff in convergence between the edge of the simulation and the zero padding was reduced. Still, this drop off is not perfect, so more work into smoothing out the edge of the simulation would prevent harsh edges when calculating the Fourier transforms.

Next, while 60 simulations of more realistic galaxy cluster lenses is an improvement over simple lens mass cases, most of the simulations look very similar and do not fully encapsulate the wide range of shapes found in galaxy clusters. Thus, more research to increase the realism of these images needs to be done.

In particular, many of the images displayed in the *Results* section are quite grainy, which is not realistic to observed galaxy clusters. To reduce this, an attempt at using a smoothing package for the mass distribution was made, but eventually abandoned since the packages we tried were not able to smooth out the images without removing fine structure within the simulations. To improve the realism of the images, future research should look for methods of smoothing that preserve detail at locations of higher mass density.

To integrate these shear plots with the analysis pipeline, the next step is to generate random mock background sources and calculate how they would appear when lensed by a foreground BAHAMAS galaxy cluster lens. This should be done by randomly generating ellipses of various redshifts, ellipticities, sizes, and orientations and then using the repository to calculate the shear and magnification at each of these background sources. Then, these stretched and magnified background sources should be displayed over an image of its associated foreground lens. The foreground lens should only have its visible particles plotted (ie., the stars).

These plots of the simulated galaxy clusters with lensed background sources overtop are the final goal of producing a mock image that can be fed into the simulation.

Acknowledgements. I'd like to thank my co-mentors Dr. Andrew Robertson, JPL, and Dr. Eric Huff, JPL, for their tremendous support on this project. Through their guidance, I was able to learn python in an approachable, exciting way and greatly look up to the way they approach physics. Additionally, I would like to sincerely thank Edward C. Stone for his generous donation to help fund my project. Without his support, I would not have been able to complete any of the work I did. I would also like to give a special thanks to the Dark Sector group at JPL and the JPL Education office for providing a community in astrophysics and connecting me with fellow mentors. Finally, thank you to my fellow interns for making the office a fun place to be and exchanging many riddles.

References

- Bartelmann, Matthias (2010). Gravitational Lensing. *Classical and Quantum Gravity*, 27(3). <https://doi.org/10.48550/arXiv.1010.3829>.
- Gravitational Lensing Formalism. (2023, June 28). In Wikipedia. https://en.wikipedia.org/wiki/Gravitational_lensing_formalism
- McCarthy, I., Schaye, J., Bird, S., & Le Brun, A., (2017). The BAHAMAS Project: Calibrated Hydrodynamical Simulations for Large-Scale Structure Cosmology. *Monthly Notices of the Royal Astronomical Society*, 465(3), 2936–2965. <https://doi.org/10.1093/mnras/stw2792>.
- Narayan, R., Barelmann, M., (1996). Lectures on Gravitational Lensing. arXiv:astro-ph/9606001.
- Romualdez, J., et al., (2018). Overview, Design, and Flight Results from SuperBIT: a High-Resolution, Wide-field, Visible-to-Near-UV Balloon-Borne Astronomical Telescope. *Ground-Based and Airborne Instrumentation for Astronomy VII*. <https://doi.org/10.48550/arXiv.1807.02887>.
- Shaaban, M. et al. (2022). Weak Lensing in the Blue: a Counter-Intuitive Strategy for Stratospheric Observations. *The Astronomical Journal*, 164(6). <https://doi.org/10.48550/arXiv.2210.09182>.